metals

MDPI

Article

Effect of Heat Treatment on Microstructure and Tensile Property of Ti-6Al-6V-2Sn Alloy

Qirui Wang [1,2], Xiaofei Lei [2], Ming Hu [2], Xin Xu [3,*], Rui Yang [2] and Limin Dong [2,*]

[1] School of Materials Science and Engineering, University of Science and Technology of China, Shenyang 110016, China; qrwang19s@imr.ac.cn
[2] Shi-changxu Innovation Center for Advanced Materials, Institute of Metal Research, Chinese Academy of Sciences, Shenyang 110016, China; xflei@imr.ac.cn (X.L.); mhu@imr.ac.cn (M.H.); ryang@imr.ac.cn (R.Y.)
[3] School of Materials, Sun Yat-Sen University, Shenzhen 518107, China
* Correspondence: xuxin58@mail.sysu.edu.cn (X.X.); lmdong@imr.ac.cn (L.D.)

Abstract: The microstructure and tensile properties of Ti-6Al-6V-2Sn alloy heat-treated at different solution and aging temperatures has been systematically investigated. Specimens were solution-treated at 970 °C (above the β transus) and 920 °C (below the β transus), respectively, followed by water quenching. When the alloy is quenched from 970 °C, α′ (hcp) and α″ (orthorhombic) martensite phases co-exist in the microstructure. When it is quenched from 920 °C, α′ martensite phase does not form, while equiaxial primary α (α_p) phase and α″ are found in the microstructure. The results also show that the strength of the alloy increases but the ductility deteriorates as the solution temperature becomes higher when the aging treatment is unchanged. This is because the volume fraction of equiaxial α_p phase is lower but the volume fraction of the acicular secondary α (α_s) phase is higher for higher solution temperature. When the alloy is aged at different temperatures after the solution treatment at 900 °C, the strength of the alloy decreases with the increase of aging temperature and the ductility shows the opposite trend as the size of the acicular α_s becomes longer and its volume fraction is lower at higher aging temperature.

Keywords: Ti-6Al-6V-2Sn; titanium alloy; heat treatment; microstructure

check for updates

Citation: Wang, Q.; Lei, X.; Hu, M.; Xu, X.; Yang, R.; Dong, L. Effect of Heat Treatment on Microstructure and Tensile Property of Ti-6Al-6V-2Sn Alloy. *Metals* **2021**, *11*, 556. https://doi.org/10.3390/met11040556

Academic Editor: Andrey Belyakov

Received: 3 March 2021
Accepted: 24 March 2021
Published: 29 March 2021

Publisher's Note: MDPI stays neutral with regard to jurisdictional claims in published maps and institutional affiliations.

Copyright: © 2021 by the authors. Licensee MDPI, Basel, Switzerland. This article is an open access article distributed under the terms and conditions of the Creative Commons Attribution (CC BY) license (https://creativecommons.org/licenses/by/4.0/).

1. Introduction

Two-phase α + β titanium alloys have been commonly used in aerospace, automotive, energy, biomedical, and other industries due to its high specific strength, excellent fatigue, and corrosion resistance [1,2]. Ti-6Al-6V-2Sn alloy, as one of typical two-phase titanium alloy, developed from Ti-6Al-4V has very good comprehensive performance and machinability, which is used for aircraft fuselage, rocket engine parts, and aerospace fasteners [3,4]. Compared to Ti-6Al-4V, Ti-6Al-6V-2Sn has more β stable elements with better hardenability and higher application temperature. Similar to Ti-6Al-4V, it shows a good response to heat treatment [5,6]. Bimodal microstructure usually endows α + β Ti alloys with good mechanical properties, which is vital for the application of the alloys [7]. Heat-treatment temperature has great influence on the formation and decomposition of metastable phases, which have significant impact on the finial microstructure and, thus, the properties of the alloys [8]. In order to obtain proper bimodal microstructure and optimized properties, appropriate solution and aging treatments are demanded. Improving the comprehensive properties of Ti-6Al-6V-2Sn alloy by heat treatment can assist the lightweight concepts in the design of Ti components, which reduces their environmental impacts and the manufacturing costs. [9].

In recent years, for Ti-6Al-6V-2Sn alloy, the element partitioning and phase transformation during continuous heating [10,11] and notched fracture behavior have been studied [12]. How heat treatments affect the bimodal microstructure of Ti-6Al-6V-2Sn alloy and its mechanical properties is still not completely clear. Therefore, the aim of this work

is studying the effect of solution and aging treatments on the microstructure and tensile properties of Ti-6Al-6V-2Sn alloy. The influence of the phase composition, microstructure morphology, size, and the volume fraction of the primary α (α_p) phase on the mechanical properties of Ti-6Al-6V-2Sn alloys has been investigated in detail. This study can deepen the understanding of the relationship of heat treatment—-microstructure—-tensile property of the alloy, which can assist the manufacturing of high-performance components, e.g., fasteners, using Ti-6Al-6V-2Sn alloys and expand the alloy's application.

2. Materials and Methods

The nominal composition of the alloy used in this study was Ti-6Al-6V-2Sn-0.5Fe-0.5Cu. Ti sponge, pure Al, Fe and Cu elements, TiO_2, Al-V alloy, and Ti-Al alloy were used to prepare the alloy in a vacuum consumable electrode melting furnace. In order to obtain a homogenous composition, the alloy was melted three times. The chemical composition of the alloy is shown in Table 1. The composition analysis standards followed were ASTM E1941 for the carbon content, ASTM E1409 for the oxygen and nitrogen contents, and ASTM E2371 for other elements' contents. The ingots were deformed into rods with a diameter of 6 mm using cogging, forging, rolling, and wire drawing. The β-transus temperature measured by the metallographic method was approximately 960 °C. The original materials were divided into three groups. Specimens in the first group (group 1) were solution-treated at 920 °C (below the β-transus, referred to as SA) and 970 °C (above the β-transus, referred to as SB) for 1 h, respectively, followed by water quenching (WQ). Specimens in the second group (group 2) were solution-treated at 800, 860, 890, 920, 950 and 970 °C for 1 h, respectively, and then water-quenched. These specimens were then aged at 540 °C for 4 h and air-cooled (AC) to room temperature and are referred to as 800, 860, 890, 920, 950, and 970. Specimens in the third group were all solution-treated at 900 °C, followed by water quenching, and then aged at 480, 500, 520, 540, 550 and 560 °C for 4 h, respectively, and air-cooled to room temperature. These specimens are referred to as 480, 500, 520, 540, and 560. All heat treatments were done in the ambient atmosphere. The oxide layers were removed during sample preparation. It is worth noting that all specimens used for microstructure characterization and tensile tests were extracted from the same stock of the alloy. Experimental scheme of heat treatment is shown in Table 2.

Zeiss AxioCam MRc5 optical microscope (OM) (Carl Zeiss Microscopy Deutschland GmbH, Oberkochen, Germany) and FEI Inspect F50 field emission scanning electron microscope (FE-SEM) (ThermoFisher Scientific, Hillsboro, OR, USA) were used for microstructure observation. Metallographic samples for OM and SEM were prepared via grinding using sandpapers and polishing using 0.02-μm colloidal silica solution. They were etched by the Kroll's etchant. The etchant ($HF:HNO_3:H_2O$ = 5:10:85) used for SA and SB specimens was more concentrated than that ($HF:HNO_3:H_2O$ = 2:2:96) for specimen groups 2 and 3 as SA and SB specimens were quenched from solution temperatures [13]. The FEI Tecnai G2 20 transmission electron microscope (TEM) (ThermoFisher Scientific, Hillsboro, OR, USA) was used to observe the microstructure and assist the analysis of the metastable phase transformation. TEM samples were ground to a thickness of about 50 μm using sandpapers. Then the samples were thinned to about 10 μm in a GATAN 656 high-precision pit-thinning instrument with a stereo microscope (Gatan Inc., Pleasanton, CA, USA). They were then ion-thinned in a GATAN PIPS II 695 precise ion-thinning instrument (Gatan Inc., Pleasanton, CA, USA). During ion thinning, the angle of ion gun was 8° and the working voltage was 4.5 KeV at the initial stage. When a bright hole was observed by the microscope, the angle of ion gun was reduced to 4° and the working voltage dropped to 1 KeV.

The qualitative analysis of phases was carried out using X-ray diffraction (XRD). All the measurements were done on a Rigaku Smartlab equipment (Rigaku Corporation, Tokyo, Japan).

The tensile tests were carried out on a SHIMADZU AG-Xplus TSE504D electronic universal testing machine (Shimadzu Corporation, Kyoto, Japan). The standard cylindrical tensile samples with a gauge length of 15 mm and a gauge diameter of 3 mm were prepared

according to the national standard GB/T228-2010. In the test, the yield strength $Rp_{0.2}$, ultimate tensile strength R_m, reduction of area Z%, and elongation A% were measured. An extensometer was used during the tests.

Table 1. The chemical composition of the alloy used in this work.

Element	Al	V	Sn	Cu	Fe	C	O% (m/m)	N% (m/m)	Ti
Content (%)	5.6	5.5	2.02	0.46	0.54	0.022	0.155	0.090	Bal.

Table 2. Heat treatments of specimens.

Group	Specimen Code	Heat Treatment
1	SA	920 °C × 1 h, WQ
	SB	970 °C × 1 h, WQ
2	800	800 °C × 1 h, WQ + 540 °C × 4 h, AC
	860	860 °C × 1 h, WQ + 540 °C × 4 h, AC
	890	890 °C × 1 h, WQ + 540 °C × 4 h, AC
	920	920 °C × 1 h, WQ + 540 °C × 4 h, AC
	950	950 °C × 1 h, WQ + 540 °C × 4 h, AC
	970	970 °C × 1 h, WQ + 540 °C × 4 h, AC
3	480	900 °C × 1 h, WQ + 480 °C × 4 h, AC
	500	900 °C × 1 h, WQ + 500 °C × 4 h, AC
	520	900 °C × 1 h, WQ + 520 °C × 4 h, AC
	540	900 °C × 1 h, WQ + 540 °C × 4 h, AC
	550	900 °C × 1 h, WQ + 550 °C × 4 h, AC
	560	900 °C × 1 h, WQ + 560 °C × 4 h, AC

3. Results

3.1. Qualitative Analysis of Phases

Figure 1 shows the XRD patterns of the Ti-6Al-6V-2Sn alloys after different heat treatments. Figure 1a shows the XRD pattern of specimen SA, which was quenched after solution treatment at 920 °C (below the β-transus). Diffraction peaks of α phase and orthorhombic martensite α″ phase can be seen, which indicates the presence of α phase and α″ phase in the specimen. Peaks of hexagonal α′phase can hardly be seen in Figure 1a, which implies that α′ phase may not form in the specimen. However, this could also be due to that the crystal structures of α and α′ phases are very similar with slightly different lattice constants and peaks of α′ phase may be covered by those of α phase. Therefore, the presence of α′ phase cannot be determined from Figure 1a and TEM is needed. TEM results will be shown in the following sections. Figure 1b is the XRD pattern of specimen SB, which was quenched from 970 °C above the β-transus. The magnified figure in Figure 1b corresponds to the marked part. As can be seen, the specimen is composed of α′ and α″ phases. Figure 1c shows the XRD patterns of the specimens in the group 2. Diffraction peaks of all specimens indicate that they consist of α and β phases. Figure 1d shows the XRD patterns of the specimens in the group 3. Their XRD patterns also show that they are composed of α and β phases. These experimental results indicate that the Ti-6Al-6V-2Sn alloy structure is composed of α and β phases after solution and aging heat treatments.

3.2. Microstructure

Figure 2 shows the OM images of the specimens SA and SB. The effect of solution temperature on the microstructure of Ti-6Al-6V-2Sn is fairly obvious. As shown in Figure 2a, the microstructure of SA sample is composed of equiaxed α_p phase and acicular α″ phase produced by incomplete lattice shear during the rapid cooling process. Volume fraction of α_p phase is about 14.3% and fine acicular martensite can be found via TEM, as shown in Figure 3a,c. Figure 2b shows the microstructure of specimen SB. The α phase has totally disappeared and the interior of the original β phase contains long, straight, acicular

martensite with staggered distribution and tiny, short martensite. Generally, α' phase is longer and thicker than α'' phase. However, it is unreliable to determine these phases by only observing this figure, and other characterization methods are needed. Density and size of the acicular phase within different original β grains varies greatly. The size of the acicular phase in some β grains is relatively long, about 60 μm. However, the size of the acicular phase inside other β grains ranges from about 20 μm to only a few microns. Orientation of the long axis of some acicular phases at the interior of β grains is crisscross. However, the acicular phases at the grain boundary are roughly parallel to each other.

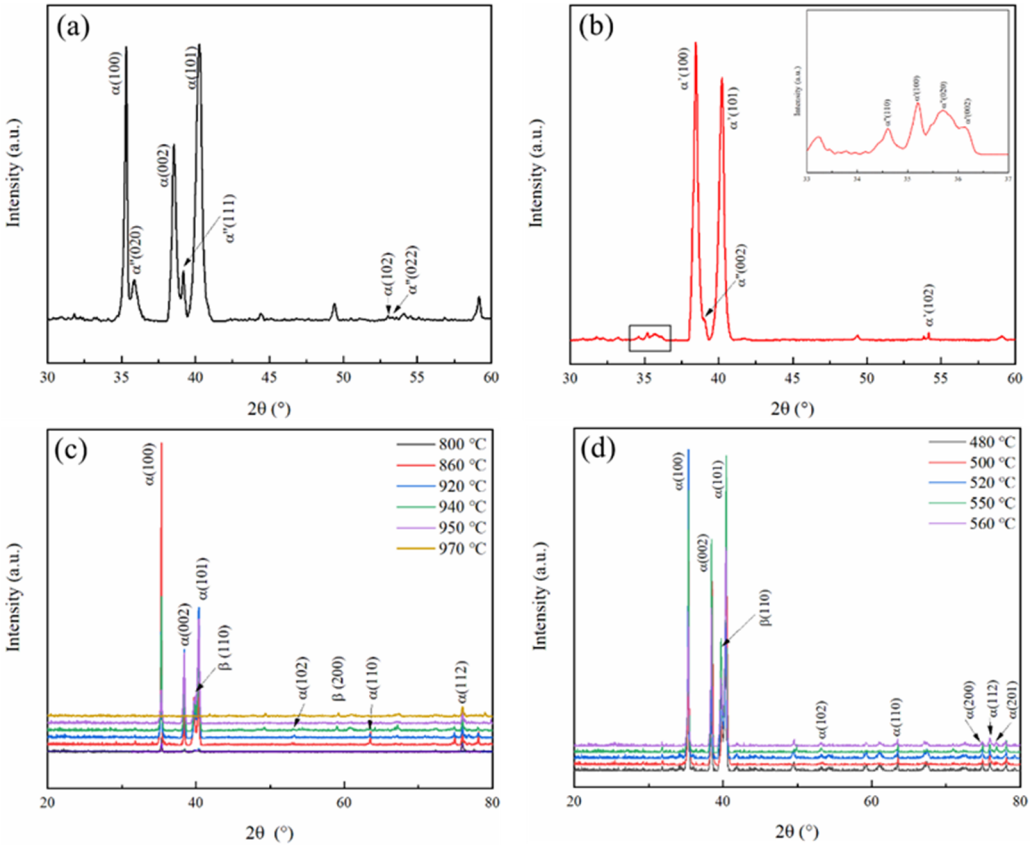


Figure 1. XRD patterns of (**a**) specimen SA solution-treated at 920 °C, (**b**) specimen SB solution-treated at 970 °C, (**c**) specimens in the group 2, 800, 860, 890, 920, 950, 970 and (**d**) specimens in the group 3, 480, 500, 520, 550, 560.

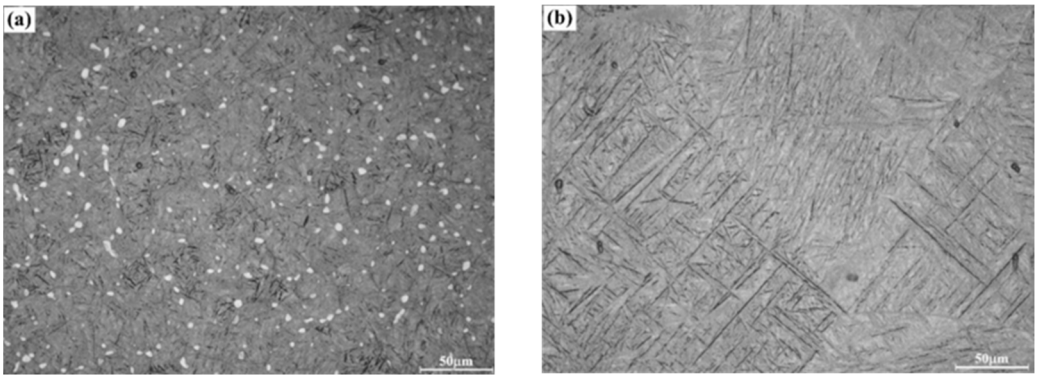


Figure 2. Optical microscopic images of Ti-6Al-6V-2Sn specimens: (**a**) SA and (**b**) SB.

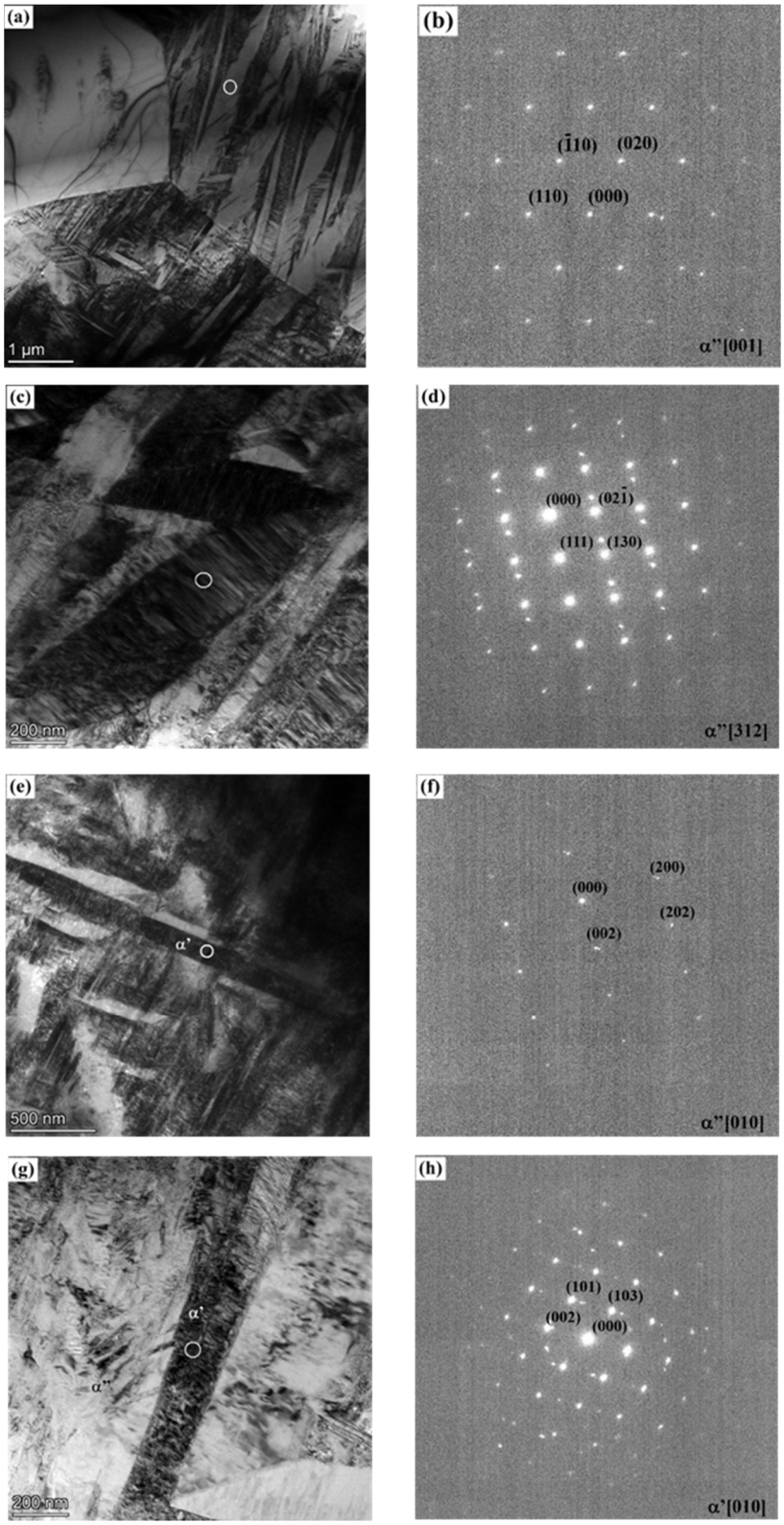


Figure 3. TEM bright field images of Ti-6Al-6V-2Sn alloy as-quenched specimens. (**a**,**c**) For specimen SA, which was water-quenched after solution treatment at 920 °C. (**e**,**g**) For specimen SB, which was water-quenched after solution treatment at 970 °C. (**b**,**d**) are the electron diffraction patterns of the areas indicated by the white circles in (**a**,**c**), respectively. The selected zone axes are α'' [1] and α'' [312], respectively. (**f**,**h**) are the electron diffraction patterns of the areas indicated by the white circles in (**e**,**g**), respectively. The selected zone axes are α'' [10] and α' [10], respectively.

Figure 3 shows TEM results of specimens SA (Figure 3a−d) and SB (Figure 3e–h). For the specimen SA, Figure 3a shows the triple-junction boundary between equiaxial α_p phase and original β grains in which martensite α'' phase can be seen. The size of α'' phase ranges from a few microns to tens of microns. A few of α'' phases run through the β grain boundary. The reason is that the grains at both sides of the grain boundary tend to be consistent in grain orientation, stacking fault, and substructure orientation such that the grain boundary has little potential to be a barrier for martensite growth [14]. The diffraction pattern of the β matrix is shown in Figure 3b. In Figure 3c, one can see a α'' phase lamella with a length of about 2 μm and a thickness of about 300 nm. Some fine secondary α'' and twins are distributed inside it, which can be proved by the diffraction pattern in Figure 3d. This may indicate that fine secondary α'' martensite phases nucleate and grow in the lamellar primary α'' martensite during rapid cooling. The growth of secondary α'' martensite can promote the generation of deformation twins, therefore increasing other nucleation sites of the secondary α'' [9]. The α' phases were not observed in the specimen SA, which may confirm that α' phase does not form in the specimen as the XRD results indicate, while, α' phase forms in specimen SB, as shown in Figure 3e–h. It can be seen from Figure 3e,g that α' phase in specimen SB seems longer but thinner than α'' phase in specimen SA. The α' phase in specimen SB has a length of about 3 μm and a thickness of about 160 nm in Figure 3e. Lamellar α'' phase also forms in specimen SB, which is illustrated in Figure 3g. Comparing Figure 3c,g, it can be found that α'' in specimen SB is much smaller than in specimen SA. In other words, the size of α'' phase coexisting with β matrix and α_p phase is obviously larger than that of α'' phase coexisting with α' in β matrix, which may be due to the different quenching temperatures and the different contents of β stabilizers in the original β grain [15].

Figure 4 shows the SEM images of specimens in group 2. As is shown in Figure 4a–e, their microstructure consists of equiaxed α_p phase (black), β phase (grey), and acicular secondary α_s phase when the solution temperature is below 950 °C. Figure 4f shows the microstructure of the aged specimen after the solution treatment at 970 °C, which is composed of only β phase and acicular α_s phase. The volume fraction variation of α_p phase is shown in Figure 5. The volume fraction of the α_p phase decreases gradually with increase of the solution temperature, and the α_p phase completely disappears when the solid solution temperature exceeds the β-transus. Nonetheless, with the increase of the solution temperature, it seems that the size and morphology of the α_p phase do not change obviously, while the acicular α_s phase is thicker and longer when the solution temperature is higher. In fact, solution temperature also determines the ratio of the volume fraction of martensite and β phase, which will have great influence on the mechanical properties of the alloy after aging.

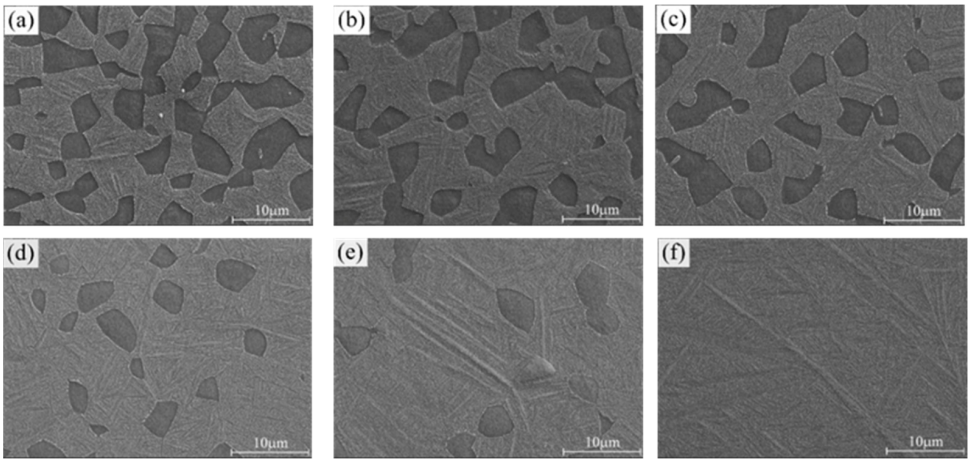


Figure 4. SEM images of Ti-6Al-6V-2Sn alloy specimens in group 2: (**a**) 800; (**b**) 860; (**c**) 890; (**d**) 920; (**e**) 950; (**f**) 970.

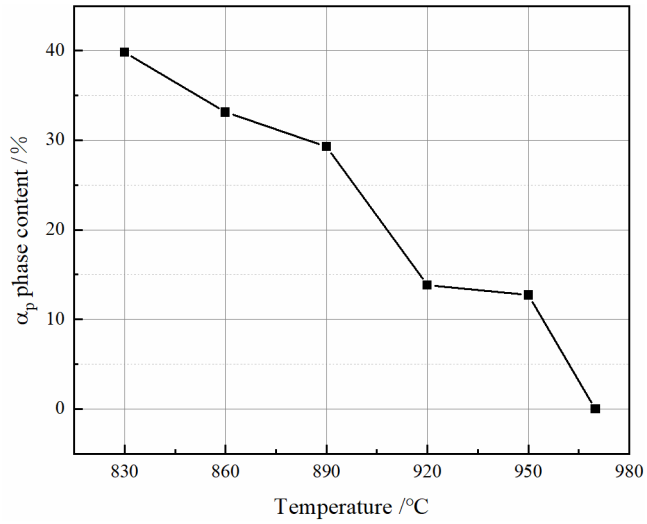


Figure 5. Evolution of the volume fraction of α_p phase as a function of solution temperature.

Figure 6 shows the microstructure of the specimens in group 3. It could be observed that the microstructure after solution and aging treatments is composed of equiaxed α_p phases, acicular α_s phase, and β phase. The equiaxed α_p phase forms during the solution treatments. The α_s phase forms during the aging treatments due to the element redistribution and martensite phase decomposition. The size and volume fraction of α_p phase seem not change with the increase of aging temperature, while the acicular α_s phase becomes thicker and longer. The α_s phase in Figure 6f is significantly thicker and longer than that in Figure 6a. This is due to the lack of decomposition driving force of the martensite phase in the aging process and the slow kinetics of the precipitation of α_s phase from β matrix when the aging temperature is low [16].

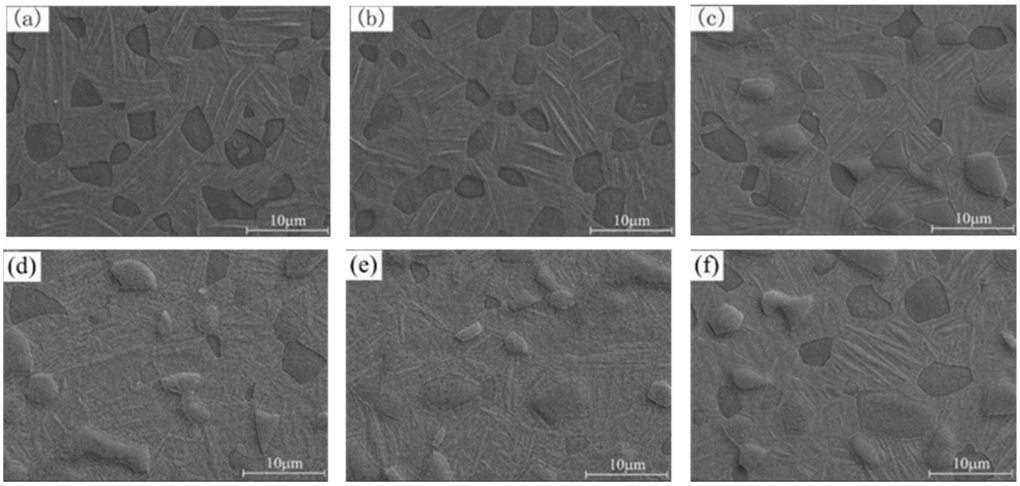


Figure 6. SEM microstructure of Ti-6Al-6V-2Sn alloy specimens in group 3: (**a**) 480, (**b**) 500, (**c**) 520, (**d**) 540, (**e**) 550, and (**f**) 560.

3.3. Tensile Properties

Figure 7a shows the evolution of the tensile properties of Ti-6Al-6V-2Sn alloy specimens in group 2, solution-treated at various temperatures and aged. As can be seen, the strength of the Ti-6Al-6V-2Sn alloy increases and the ductility decreases with the increase of solution temperature when the aging condition is constant. When the solution temperature reaches 950 °C, the strength reaches the maximum and the yield strength and tensile strength are 1457 MPa and 1539 MPa, respectively. However, the ductility is relatively poor

as the elongation is only 3.5% and reduction of the area is only 9%. When the solution temperature is over 960 °C (β-transus), both strength and ductility decrease and brittle fracture happens. This is due to the disappearance of equiaxed α_p phase, which can be seen from Figure 4f, and the β grains tend to grow up in the β-phase region. The coarsening of β grains can cause a sharp drop of ductility. When the solution temperature is between 900 °C and 930 °C, the strength and ductility of the alloy are relatively balanced. Figure 7b shows the engineering stress–strain curves of the specimens in group 2 and indicates the same trend as described above.

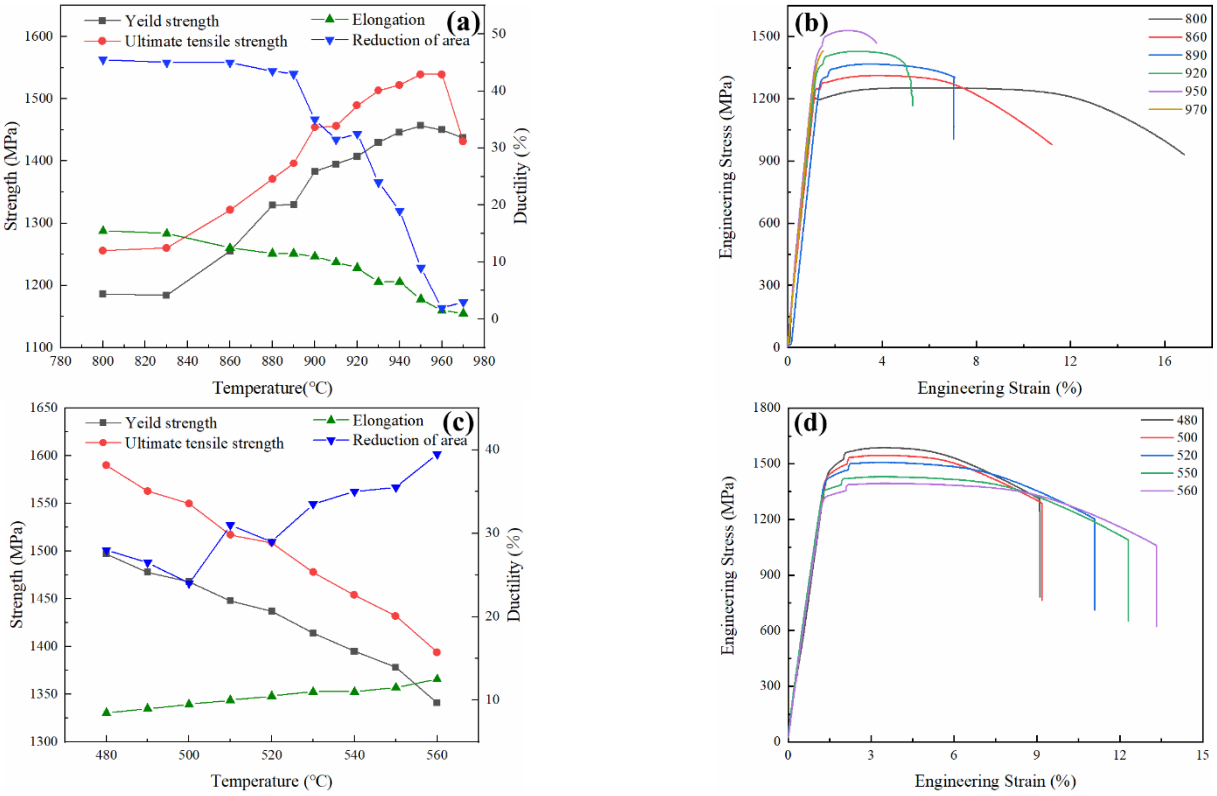


Figure 7. (**a**) Tensile properties and (**b**) the engineering stress–strain curves of Ti-6Al-6V-2Sn alloy solution treated at different temperatures and then aged at 540 °C for 4 h (group 2); (**c**) tensile properties and (**d**) the engineering stress–strain curves of Ti-6Al-6V-2Sn alloy solution treated at 900 °C and then aged at different aging temperature for 4 h (group 3).

Figure 7c shows the variations in the tensile properties of Ti-6Al-6V-2Sn alloy specimens in group 3, solution-treated at 900 °C and aged at different temperatures. As shown in the figure, the strength of the alloy decreases with the increase of the aging temperature, while the ductility increases. When the aging temperature is 480 °C, the strength reaches the maximum and the yield strength and tensile strength are 1497 MPa and 1590 MPa, respectively. However, the ductility is poor, as the elongation is 8.5% and the reduction of area is only 28%. The strength and ductility are relatively balanced at the aging temperature of 520 °C. The yield strength and tensile strength are 1437 MPa and 1509 MPa, respectively, and the ductility is better than that of specimen 480. The best ductility is achieved at 560 °C, with an elongation of 12.5% and a reduction of area of about 39.5%, but the strength is the lowest with a yield strength of 1341 MPa and a tensile strength of 1394 MPa. The engineering stress–strain curves of the specimens in group 3 are shown in Figure 7d and it indicates the same trend as described above. The mechanical properties are closely related to microstructure, especially the morphology and size of α_s phase. When the aging temperature is low, for example, 480 °C, α_s phase is easy to nucleate, but the diffusion of elements is slow and it is difficult for α_s phase to grow up. As a result, dispersed α_s phase is fine and dense. Therefore, the alloy strength is high but the ductility is low. With the

increase of aging temperature, the coarsening of acicular α_s phase occurrs and, thus, the strength decreases but the ductility becomes better [17].

3.4. Fracture Morphology

Figure 8 shows fracture morphology of tensile samples in the group 2, which were solution-treated at different temperatures and aged at 540 °C. It can be seen from Figure 8a–d that the samples underwent necking before fracture when the solution temperature was 800–920 °C. The fracture surfaces consist of fibrous zones, radiation zones, and shear lips. A large number of dimples and tiny holes can be observed at higher magnifications, indicating ductile fracture. The dimple size increases slightly with the increase of solution temperature, indicating that the samples become less ductile. According to Figure 8e, when the solution temperature reaches 950 °C, the shear lip disappeares. Elongated dimples, dissociation steps, and tearing edges are present at the fracture surface. The results show that the sample becomes brittle and plastic deformation is localized. Figure 8f shows that when the solution temperature is higher than the phase transition point (~960 °C), reaching 970 °C, the fracture surface shows dissociation steps formed by parallel dissociation planes at different heights. The dissociation steps constitute the river pattern. The development direction of the river pattern indicates the direction of the crack propagation, and the crack source is found at the initial point of the river pattern, as indicated by the arrow in Figure 8f. Therefore, the 970 sample underwent a brittle fracture.

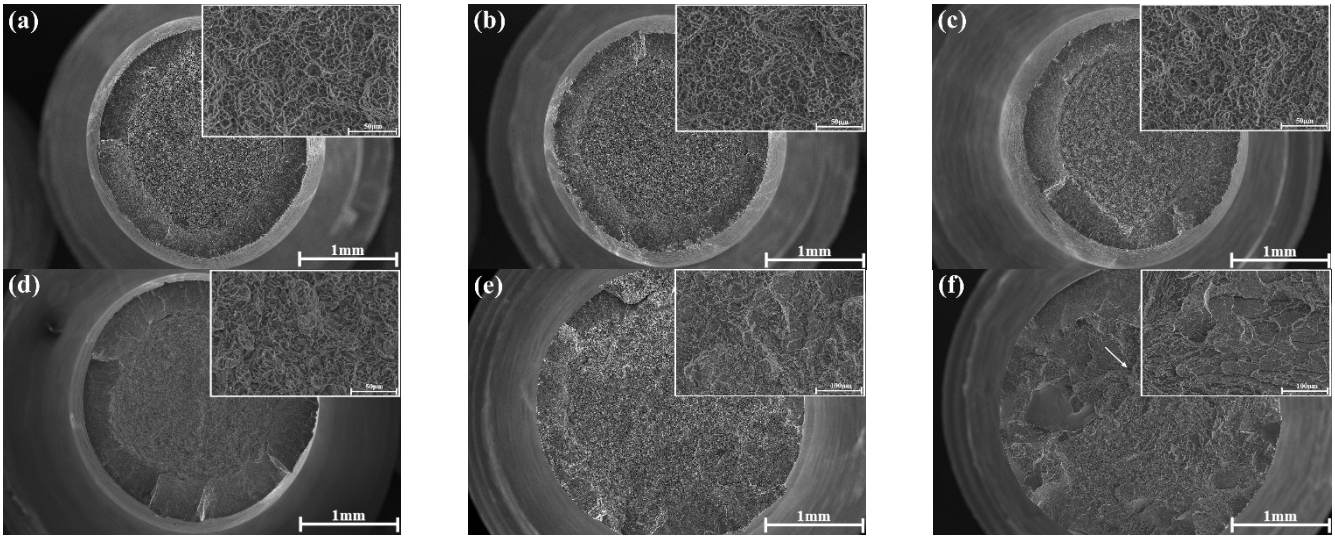


Figure 8. Fracture morphology of tensile samples solution-treated at (**a**) 800, (**b**) 860, (**c**) 890, (**d**) 920, (**e**) 950, and (**f**) 970 °C for 1 h and aged at 540 °C for 4 h.

Figure 9 shows the fracture morphology of tensile samples in the group 3, which were solution-treated at 900 °C and then aged at different temperatures. It can be seen that the fracture surface of all samples is composed of fibrous zones, radiation zones, and shear lips. The dimple is mainly equiaxial and the crack source is at the center of the fibrous zone. The dimples and micropores have little difference in size. There are tear edges and detachment steps in the radiation zone, which are formed by rapid tearing with low energy and have the characteristics of the radiation pattern parallel to the direction of crack propagation [18]. These features indicate that the samples underwent ductile fracture during tensile tests.

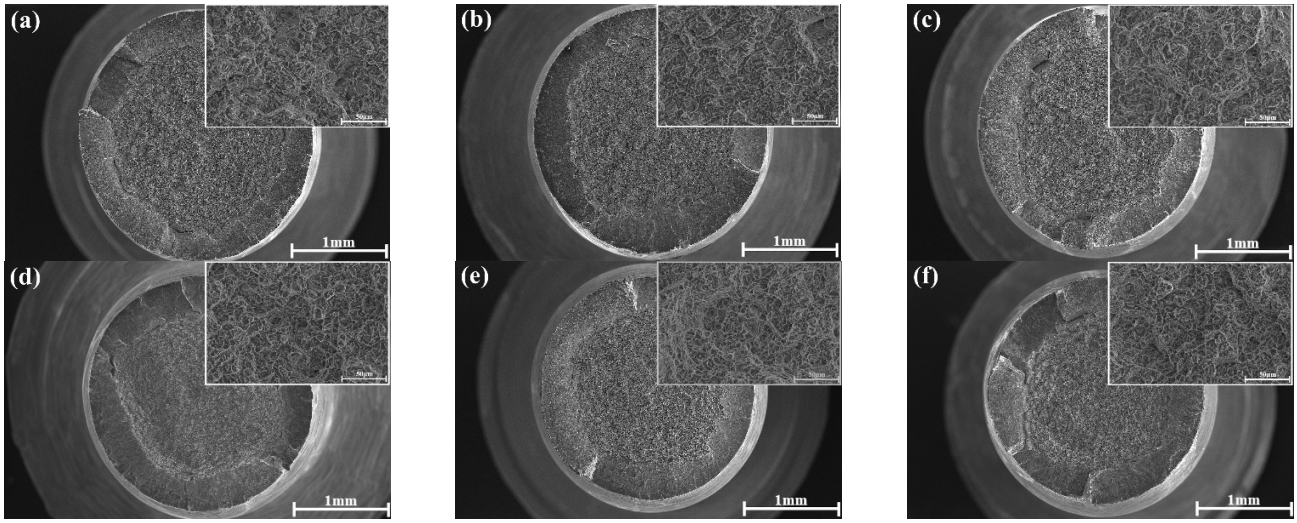


Figure 9. Fracture morphology of tensile samples solution-treated at 900 °C for 1 h then aged at different temperatures for 4 h: (**a**) 480, (**b**) 500, (**c**) 520, (**d**) 540, (**e**) 550, and (**f**) 560 °C.

4. Discussion

4.1. Effect of Solution Temperature for the As-Quenched Conditions

For solution-treated and quenched Ti-6Al-6V-2Sn alloy, the phases formed after quenching are closely related to the solution temperature and the composition of β phase. Results show that, when the alloy is solution-treated at 970 °C, α′ and α″ martensite form in the alloy after quenching. However, when the alloy is solution-treated at 920 °C and quenched, only α″ martensite forms during quenching. The size of α″ in specimen SB is smaller than that in specimen SA and also smaller than the size of α′ in specimen SB. The α″ can be seen as a transitional phase between α′ and β [19,20]. From the perspective of thermodynamics, high solution temperature leads to strong martensite phase transformation driving force during quenching in Ti alloys. Therefore, the transformation driving force is larger when quenching from 970 °C and there could be enough driving force to transform β to α′. Consequently, both α′ and α″ form in specimen SB. From the perspective of the composition of β phase [21], higher β stabilizer contents hinder the transformation from β to α′. When the alloy is solution-treated at 920 °C below the β-transus, α_p phase precipitates in the alloy and it absorbs α stabilizers from β phase and rejects β stabilizers into β phase. As a result, the content of β stabilizers in the β phase becomes higher and the lattice transition resistance increases during the martensite transformation. β to α′ cannot occur and only α″ forms after quenching.

The α′ martensite forming after water-cooling has a considerable strengthening effect in the alloy, but the ductility of the alloy decreases dramatically with the amount of α′ increasing [22,23]. However, it has been reported that α″ phase has a softening effect [24]. Therefore, one way to improve the mechanical properties of the alloy is decomposing α′ and α″ into fine and dispersive α_s and β phase. This is one of the aging strengthening mechanisms of Ti-6Al-6V-2Sn alloy.

4.2. Effect of Heat-Treatment Temperature for the Aged Conditions

Three factors play vital roles in the heat-treatment strengthening mechanism of Ti alloys [25]. The first and most important one is the number of dispersive α phases transformed from the martensite during aging, which mainly depends on quenching temperature and aging temperature. The second one is the hardness and elastic properties of the α phase which can affect the strengthening effect. The α stabilizers can improve the hardness and elastic properties of α phase. The third one is the morphology and particle size of the α phase. For example, equiaxial α_p particles could improve ductility compared to the staggered small acicular α_s. While, the latter can enhance the strength of the alloy.

The influence of solution temperature and aging temperature on the phase composition, morphology, and size of phases is obvious. Figure 7a shows that the strength of the alloy increases but the ductility decreases with the increase of solution temperature. Figure 8 shows that with the increase of solution temperature, the fracture mode of the alloy changes from ductile fracture to brittle fracture, and the transition point is near the β-transus. This is because the volume fraction of equiaxed α_p phase decreases with the increase of solution temperature and, thus, the volume fraction of fine acicular α_s increases after aging at a certain temperature, as shown in Figure 4. Furthermore, quenching from higher solution temperature forms more metastable phases (α'', α') which decompose into acicular α_s phase and stable β phase during aging treatment. This can promote the precipitation of α_s. The phase interface between α_s and β hinders dislocation movement and reduces its moving space, which makes the deformation difficult and, thus, the alloy's strength improves but the ductility deteriorates. The fine acicular α_s has a strong strengthening effect. On the other hand, equiaxed α_p phase is much larger than the fine acicular α_s. Also, dislocations could move inside α_p and propagate at its grain boundaries. Therefore, the equiaxial α_p phase can help accommodate deformation and improve the ductility [26]. As a consequence, increasing the solution temperature enhances the strength of the alloy but decreased its ductility when the aging treatment condition is unchanged.

It can be seen from Figure 7c that the strength of the alloy decreases with the increase of aging temperature for the same solution-treatment condition. Figure 9 shows that the alloy experienced ductile fracture when it was aged at different temperatures. As is known, in the two-phase region, the equilibrium α phase fraction is higher at lower aging temperature, which indicated higher volume fraction of α_s for samples solution-treated at a certain temperature before aging. Moreover, the growth of α_s is slower at lower aging temperature, meaning finer α_s. Consequentially, lower aging temperature could produce very dense and fine α_s in the β matrix, as indicated in Figure 6. This enhances the strengthening effect of acicular α_s, thus promoting the strength of the alloy. However, its ductility is lower. When the aging temperature increases, the acicular α_s phase becomes coarser and this benefits the toughness and crack growth resistance of the alloy.

5. Conclusions

The role of heat treatment in the microstructure and tensile property of Ti-6Al-6V-2Sn alloy has been systematically studied. This work can assist the design of heat treatment of the alloy to optimize its mechanical properties. The following conclusions can be drawn.

(1) When the alloy is solution-treated at 970 °C and water-quenched, hexagonal α' and orthorhombic α'' martensite phases form. The size of α'' is obviously smaller than α'. When the alloy is solution-treated at 920 °C and water-quenched, α' phase does not form and only α'' forms.

(2) With the increase of solution temperature, the strength of the alloy increases and the ductility decreases due to the decrease of the volume fraction of equiaxial α_p phase and the increase of the volume fraction of acicular α_s phase formed during aging. When the solution temperature is 920 °C, the strength and ductility of the alloy aged at 540 °C are relatively balanced with a yield strength of 1407 MPa, ultimate tensile strength of 1489 MPa, reduction of area of 32.5%, and elongation of 9%.

(3) With the increase of aging temperature, the strength of the alloy deteriorates and the ductility enhances, which may be due to the coarsening of α_s and its higher fraction. The mechanical properties of the alloy are optimal when the aging temperature is 520 °C with a yield strength of 1437 MPa, ultimate tensile strength of 1509 MPa, reduction of area of 29%, and elongation of 10.5%.

Author Contributions: Q.W. and L.D. conceived and designed the experiments; Q.W. performed the experiments; Q.W., X.L., M.H., L.D., X.X., and R.Y. analyzed the data and contributed to the writing; X.X. did the revision and direction. All authors have read and agreed to the published version of the manuscript.

Funding: The work was supported by the National Science Foundation for Young Scientists of China [51801199].

Institutional Review Board Statement: Not applicable.

Informed Consent Statement: Not applicable.

Data Availability Statement: Data sharing not applicable.

Conflicts of Interest: The authors declare no conflict of interest.

References

1. Wood, J.R.; Russo, P.A.; Welter, M.F. Thermomechanical Processing and Heat Treatment of Ti-6Al-2Sn-2Zr-2Cr-2Mo-Si for Structural Applications. *Mater. Sci. Eng. A Struct. Mater. Prop. Microstruct. Process.* **1998**, *243*, 109–118. [CrossRef]
2. Banerjee, D.; Williams, J. Perspectives on Titanium Science and Technology. *Acta Mater.* **2013**, *61*, 844–879. [CrossRef]
3. Wollmann, M.; Kiese, J.; Wagner, L. Properties and Applications of Titanium Alloys in Transport. Ti-2011. In Proceedings of the 12th World Conference on Titanium, Beijing, China, 19–24 June 2011; pp. 837–844.
4. Leyens, C.; Peters, M. Titanium and Titanium Alloys. Belov, J.C.W.F., Ed.; Chemical and Chemical Industry Press: Beijing, China, 2005; pp. 292–302.
5. Fujii, H. Strengthening of Alpha+Beta Titanium Alloys by Thermomechanical Processing. *Mater. Sci. Eng. A Struct. Mater. Prop. Microstruct. Process.* **1998**, *243*, 103–108. [CrossRef]
6. Boyer, R.; Welsch, G. *Materials Properties Handbook: Titanium Alloys*; ASM International: Materials Park, OH, USA, 1994; pp. 637–666.
7. Sarma, J.; Kumar, R.; Sahoo, A.K.; Panda, A. Enhancement of material properties of titanium alloys through heat treatment process: A brief review. *Mater. Today Proc.* **2020**, *23*, 561–564. [CrossRef]
8. Filip, R.; Kubiak, K.; Ziaja, W.; Sieniawski, J. The effect of microstructure on the mechanical properties of two-phase titanium alloys. *J. Mater. Process. Technol.* **2003**, *133*, 84–89. [CrossRef]
9. Ortiz, M. Investigation of Thermal-Related Effects in Hot SPIF of Ti-6Al-4V Alloy. *Int. J. Precis. Eng. Manuf. Green Technol.* **2020**, *7*, 299–317. [CrossRef]
10. Barriobero-Vila, P.; Oliveira, V.B.; Schwarz, S. Tracking the Alpha Martensite Decomposition during Continuous Heating of a Ti-6A1-6V-2Sn Alloy. *Acta Mater.* **2017**, *135*, 132–143. [CrossRef]
11. Barriobero-Vila, P.; Williams, J.C. Role of Element Partitioning on the alpha-beta Phase Transformation Kinetics of a Bi-modal Ti-6Al-6V-2Sn Alloy during Continuous Heating. *J. Alloys Compd.* **2015**, *626*, 330–339. [CrossRef]
12. Huang, R.T.; Huang, W.L.; Huang, R.H. Effects of Microstructures on the Notch Tensile Fracture Feature of Heat-treated Ti-6Al-6V-2Sn Alloy. *Mater. Sci. Eng. A Struct. Mater. Prop. Microstruct. Process.* **2014**, *595*, 297–305. [CrossRef]
13. Bolisowa, E.A. *Metallography of Titanium Alloys*; National Defense Industry Press: Beijing, China, 1980; p. 20.
14. Shao, J.J.C.S.Z. In-situ Observation of Transgranular Growth of Martensite in A Cu-Zn-Al Shape Memory Alloy. *Acta Met. Sin.* **1988**, *24*, 213–216.
15. Li, C.; Li, G.; Yang, Y.; Yang, K. Influence of Quenching Tempetrature on Martensite Type in Ti-4Al-4.5Mo Alloy. *Acta Met. Sin.* **2010**, *46*, 1061–1065. [CrossRef]
16. Zhu, B.; Zeng, W.D.; Chen, L. Influences of Solution and Aging Treatment Process on Microstructure and Mechanical Properties of Ti-6Al-6V-2Sn Titanium Alloy Rods. *Chin. J. Nonferrous Met.* **2018**, *28*, 677–684. [CrossRef]
17. Li, C.; Chen, J.H.; Wu, X. A Comparative Study of the Microstructure and Mechanical Properties of alpha plus beta Titanium Alloys. *Met. Sci. Heat Treat.* **2014**, *56*, 374–380. [CrossRef]
18. Lei, X.; Dong, L.; Zhang, Z.; Liu, Y.; Hao, Y.; Yang, R.; Zhang, L.-C. Microstructure, Texture Evolution and Mechanical Properties of VT3-1 Titanium Alloy Processed by Multi-Pass Drawing and Subsequent Isothermal Annealing. *Metals* **2017**, *7*, 131. [CrossRef]
19. Yang, R.; Saunders, N.; Leake, J.A. Euilibria and Microstructural Evolution in the Beta/Beta 'Gamma' Region of the Ni-Al-Ti System- Modeling and Experiment. *Acta Metall. Mater.* **1992**, *40*, 1553–1562. [CrossRef]
20. Ahmed, T.; Rack, H.J. Martensitic transformations in Ti-(16–26 at%) Nb alloys. *J. Mater. Sci.* **1996**, *31*, 4267–4276. [CrossRef]
21. Elmer, J.W.; Palmer, T.A.; Babu, S.S. Phase Transformation Dynamics during Welding of Ti-6Al-4V. *J. Appl. Phys.* **2004**, *95*, 8327–8339. [CrossRef]
22. Galarraga, H.; Warren, R.J.; Lados, D.A.; Dehoff, R.R.; Kirka, M.M.; Nandwana, P. Effects of heat treatments on microstructure and properties of Ti-6Al-4V ELI alloy fabricated by electron beam melting (EBM). *Mater. Sci. Eng. A* **2017**, *685*, 417–428. [CrossRef]
23. Motyka, M. Decomposition of Deformed Alpha '(Alpha') Martensitic Phase in Ti-6Al-4V Alloy. *Mater. Sci. Technol.* **2019**, *35*, 260–272. [CrossRef]
24. Zhu, Z.; Wang, Q.J.; Mo, W. *Metallography and Heat Treatment of Titanium*; Metallurgical Industry Press: BeiJing, China, 2014; p. 50.
25. Bolisowa, E.A. *Metallography of Titanium Alloys*; National Defense Industry Press: Beijing, China, 1980; pp. 191–194.
26. Chen, J.; Zhao, Y.Q.; Zeng, W.D. Influence of Primary alpha Phase on Impact Toughness of TC21 Titanium Alloy. *Rare Met. Mater. Eng.* **2006**, *35*, 174–177.